Article type: Communication

Dual-phase singularity at a single incident angle with spectral tunability in Tamm cavities

Kandammathe Valiyaveedu Sreekanth, Sambhu Jana, Qing Yang Steve Wu, Zhao Meng, Ranjan Singh and Jinghua Teng**

Dr. K. V. Sreekanth, Dr. Q. Y. Steve Wu, Dr. Z. Meng, Prof. J. Teng
Institute of Materials Research and Engineering, Agency for Science, Technology and Research (A*STAR), 2 Fusionopolis Way, Innovis #08-03, Singapore, 138634, Republic of Singapore

S. Jana, Prof. R. Singh
Division of Physics and Applied Physics, School of Physical and Mathematical Sciences, Nanyang Technological University, Singapore 637371, Singapore

S. Jana, Prof. R. Singh
Centre for Disruptive Photonic Technologies, The Photonics Institute, Nanyang Technological University, Singapore 637371, Singapore

*E-mail: sreekanth@imre.a-star.edu.sg, jh-teng@imre.a-star.edu.sg

Keywords: Thin film coatings, optical Tamm states, phase change materials, phase singularity, hydrogen sensors

Abstract

The phase singularity, a sudden phase change occurring at the reflection zero has widely been explored using various nanophotonic systems such as metamaterials and thin film cavities. Typically, these systems exhibit a single reflection zero with a phase singularity at a specific incident angle, particularly at larger angles of incidence (> 50 degrees). However, achieving multiple phase singularities at a single incident angle remains a formidable challenge. Here, we experimentally demonstrate the existence of a dual-phase singularity at a lower incident angle using a tunable Tamm plasmon polariton (TPP) cavity. The tunable TPP cavity consists of gold-coated ultralow-loss phase change material Sb_2S_3-based distributed Bragg reflector, which can excite narrowband TPP resonances from normal incidence to a wide angle of incidence for both *s*- and *p*-polarizations of light. Notably, this TPP cavity shows dual-phase singularity at lower angles of incidence since the excited TPP for *s*- and *p*-polarizations exhibits zero reflection at slightly different wavelengths for the same incident angle. To demonstrate the potential application of the dual-phase singularity, we propose a TPP cavity-based scalable hydrogen sensor and show that the dual-phase singularity can further improve the sensitivity of singular phase-based sensing approaches. Moreover, we experimentally demonstrate spectrally tunable dual-phase singularity at a lower incident angle using a metal-free Tamm cavity.

1 Introduction

Achieving phase singularity by completely suppressing the reflection of light is an emerging research area[1], especially for ultra-sensitive sensing applications[2]. For one incident angle and polarization state, an abrupt phase change occurs at the reflection zero, which has been extensively studied using different optical systems including Brewster angle [3-4], topological darkness [5], non-Hermitian systems [6, 7], excitons of two-dimensional material [8, 9], perfect absorption [10-12], prism coupled surface plasmon resonance [13-15], and Fabry-Pérot (F-P) cavities [16-20]. Among these, topological phase singularity has recently received great attention and many material systems including plasmonic gold nanoarrays [21], self-assembled plasmonic metamaterials [22], 3D plasmonic crystal metamaterial [23], metasurfaces [24, 25], photonic crystals [26] have been explored. However, these systems require intense nanofabrication steps and bulky prisms to achieve phase singularity. The lithography-free approaches including F-P cavities provide a scalable platform to realize phase singularity for cost-effective applications. However, all these systems exhibit a single-phase singularity under specific conditions, especially at a higher angle of incidence.

An attempt to achieve multiple-phase singularity is demonstrated by integrating high refractive index two-dimensional materials with the F-P resonator of SiO_2/Si substrate, using the principle of topologically protected reflection zeros[27]. Even though three-phase singularities are realized at the reflection zeros of *p*- and *s*-polarizations, they are observed at entirely different incident angles. For active control of phase singularity (on/off switch), an all-optical control is demonstrated by coating a thin film of organic molecule on Si substrate, where a weakly- to strongly-coupled regime was created to tune the reflection zeros by the reversible photoisomerization of organic molecules[28]. The requirement to observe multiple-phase singularity in these systems is that the light should be incident at a higher angle of incidence (> 50°) from the normal. This is because most of the F-P cavities are polarization-dependent and the zero reflection at the cavity resonance is only possible at a higher angle of incidence. The realization of phase singularity at a near-normal and lower incident angle is important to develop a practical sensing system, in particular, an interferometer-based differential phase imaging sensor could be realized [29]. Moreover, achieving multiple phase singularities at a single incident angle is beneficial for phase engineering in flat optics [30] as well as for improving the detection limit of sensors, where the phase singularity at different wavelengths can be simultaneously used for sensing. To achieve multiple-phase singularity at a single and lower incident angle, a narrow linewidth mode with reflection zero for both *s*- and *p*-polarizations is required at the same incident angle, which remains an unresolved problem with existing F-P cavity-based systems.

Tamm plasmon polariton (TPP) cavity, a thin metal film coated with a distributed Bragg reflector (DBR), is a scalable platform to realize narrowband plasmonic resonance for both *s*- and *p*-polarizations of light[31]. The optical Tamm states can be excited within the photonic bandgaps of DBR from the free space because the DBR provides the required optical phase matching for the TPP excitation. More importantly, the high-quality factor TPP modes can be excited from normal incidence to a wide angular range. The active control of TPP mode is also demonstrated by integrating functional materials such as liquid crystals[32], cadmium oxide[33] (CdO), and chalcogenide phase change material[34] (PCM) with DBR. In particular, the PCM-based TPP cavity shows a multi-mode response with large spectral tunability by changing the structural phase of PCM from amorphous to crystalline[34]. Owing to these reasons, Tamm cavities have been considered as a scalable plasmonic platform for a wide spectral band from ultraviolet to terahertz [35-37] and proposed for various applications including thermal emitters [38], surface-enhanced Raman spectroscopy [33], lasers [39], and hot electron photodetectors [40]. In particular, Tamm cavities have been widely explored for high-performance refractive index sensing applications due to the strong electromagnetic field enhancement at the metal/surrounding medium interface, where a spectral shift of Tamm resonance is normally monitored when the refractive index of analyte changes [41-43]. Moreover, the optical Tamm state is also used to realize single reflection zero with one phase singularity for temperature and refractive index sensing applications [44, 45].

Here, we experimentally demonstrate optical Tamm state-induced dual-phase singularity at a single lower incident angle. To accomplish this, reflection zero for *s*-and *p*-polarized Tamm mode is obtained at the same incident angle. For this purpose, a TPP cavity made up of a gold thin film coated with an Sb_2S_3-SiO_2 DBR is developed. Due to the large refractive index contrast between Sb_2S_3 and SiO_2, fewer DBR layers are sufficient to realize narrow linewidth and zero reflection Tamm modes for *s*-and *p*-polarization at near-infrared (NIR) wavelengths. As an example of a possible application, we propose a Tamm cavity-based hydrogen sensor and numerically demonstrate that the refractive index sensitivity of ellipsometer parameters (Ψ and Δ) at the dual-phase singularity wavelength is much higher than the single-phase singularity approach. Further, we experimentally demonstrate a metal-free Tamm cavity comprising two DBRs to achieve spectrally tunable dual-phase singularity at a lower incident angle.

2 Design of TPP Cavity for Dual-Phase Singularity

Figure 1a illustrates the designed TPP cavity for realizing dual-phase singularity in reflection, consisting of a thin Au layer coated at the bottom of the Sb_2S_3-SiO_2 DBR. Among chalcogenide PCM families, Sb_2S_3 is a suitable high refractive index and lossless PCM for tunable DBR development in the NIR wavelengths [46, 47]. In particular, Sb_2S_3 shows lossless characteristics in both its amorphous and crystalline phases within the NIR wavelengths (see Supporting Information Fig. S1a). Since the refractive index contrast between Sb_2S_3 and SiO_2 is higher than the commonly used DBR materials (eg. TiO_2 and SiO_2), a lesser number of layers are sufficient to realize photonic bandgap (PBG) in the NIR wavelengths. Thus, the proposed DBR consists of 10 alternating layers of SiO_2 and Sb_2S_3 with a thickness of 100 nm and 180 nm for SiO_2 and

Sb_2S_3, respectively. To achieve zero reflection at the TPP resonance wavelength, the thickness of the Au layer and Sb_2S_3 termination layer is very crucial. In our calculations using the transfer matrix method [48], the optimized thickness of the Au layer and Sb_2S_3 termination layer are selected as 28 nm and 181 nm, respectively. The experimentally acquired optical constants of Sb_2S_3, SiO_2, and Au are used in the simulation (see Supporting Information Fig. S1). The proposed TPP cavity excites tunable Tamm mode within the PBG of DBR in the NIR wavelengths (see Supporting Information Fig. S2). As can be seen, zero reflection with a narrow linewidth, full wave at half maximum (FWHM) = 37 nm, is obtained for amorphous Sb_2S_3. However, due to a slight broadening of the linewidth of the Tamm mode (FWHM = 40 nm) and the failure to achieve zero reflection for the crystalline Sb_2S_3, we exclusively focus on the amorphous Sb_2S_3 for the demonstration of dual-phase singularity.

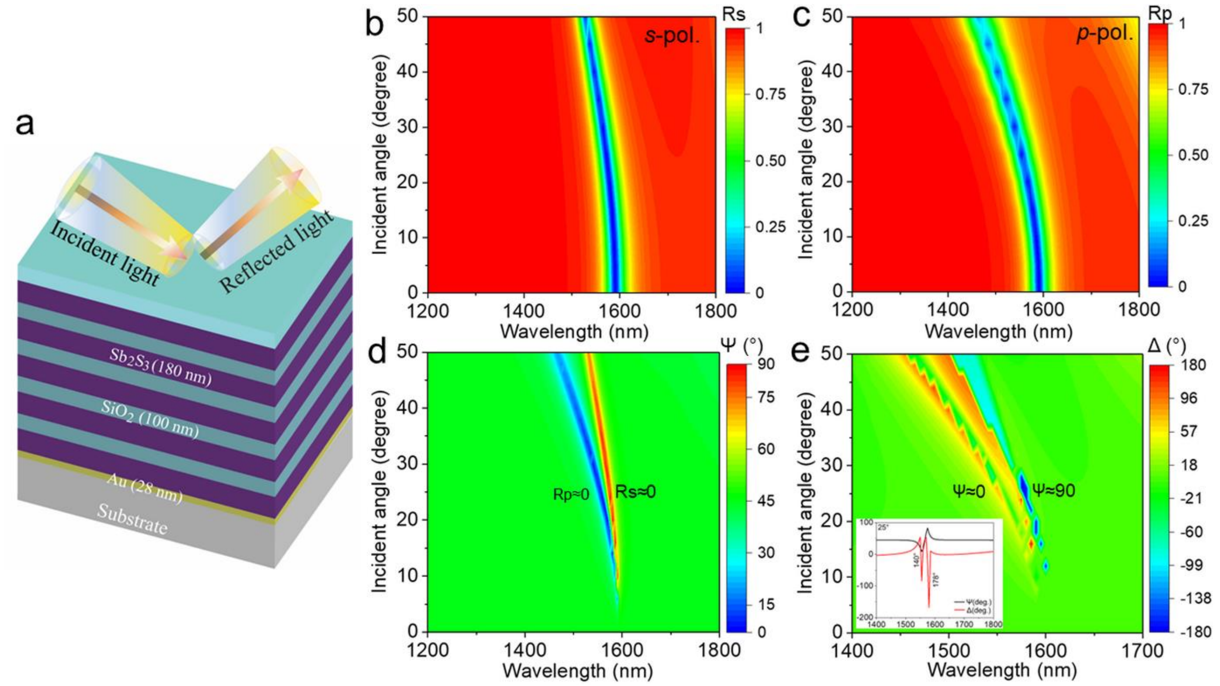

Figure 1. **Design for TPP cavity for dual-phase singularity**. (**a**) Schematic of the designed TPP cavity consisting of Sb_2S_3-SiO_2 DBR coated with Au layer. Calculated angular reflectance spectra of TPP cavity for (**b**) *s*-polarization and (**c**) *p*-polarization. (**d**) Calculated incident angle dependent ψ spectra, where the blue curve represents $\psi \approx 0$ when $R_p = 0$ and the red curve represents $\psi \approx 90$ when $R_s = 0$. (**e**) Calculated incident angle dependent Δ spectra, where yellow

(right) and blue (left) regions represent sudden phase change that occurred when ψ ≈ 0 and ψ ≈ 90, respectively. The inset of Fig. (e) shows the calculated pair of ellipsometer parameters (ψ and Δ) at 25°, where the phase singularity is exactly obtained at the minimum and maximum values of ψ.

In **Fig. 1b** and **1c**, we show the calculated angular reflectance spectra (0° to 50°) of the TPP cavity for *s*- and *p*-polarizations, respectively. Note that TPP mode spectrally overlaps for *s*- and *p*-polarizations at normal incidence and spectrally separates with increasing incident angle. For *s*-polarized reflection (R_s), a slight blue shift of Tamm resonance with almost zero reflection is obtained with increasing incident angle. However, for *p*-polarized reflection (R_p), the Tamm resonance blue shifts significantly, and the linewidth broadens with increasing incident angle. This is because the photonic bandgap of DBR for *p*-polarization shrinks with increasing incident angle, due to the Brewster effect at the interface between SiO_2 and Sb_2S_3 layers (see Supporting Information Fig. S3).

We further calculate the ellipsometer parameters (Ψ and Δ) to demonstrate the dual-phase singularity at a single incident angle. In ellipsometry, the complex reflectance of a system, ρ, is parametrized by the amplitude component Ψ and the phase difference between *s*- and *p*-polarization Δ, that is, $\rho = \frac{r_p}{r_s} = \tan\Psi e^{i\Delta}$. Here Ψ can vary from 0° to 90° in which Ψ ≈ 0 (Ψ_{min}) and Ψ ≈ 90 (Ψ_{max}) when $R_p = 0$ and $R_s = 0$, respectively. Moreover, the reflection phase undergoes a ~ π phase shift at Ψ_{min} and Ψ_{max}. Thus, the dual-phase singularity, one at Ψ_{min} and the second at Ψ_{max} is achievable at a single incident angle. The calculated Ψ and Δ spectra as a function of incident angle are shown in **Figure 1d** and **1e**, respectively. As shown in **Figure 1d**, Ψ_{min} (blue) and Ψ_{max} (red) regions spectrally overlap at smaller angles of incidence around 10° to 15° and spectrally separate with increasing incident angle. Also, with increasing incident angle (> 30°), the Ψ_{min} value increases and the Ψ_{max} value decreases. Therefore, the lowest Ψ_{min} value and highest Ψ_{max} value with abrupt phase change are possible at a lower incident angle. It is clear from **Figure 1e** that maximum phase change at Ψ_{min} and Ψ_{max} is possible at a certain incident angle ≤ 25°. Also, note from the inset of Figure 1e that phase singularity is exactly obtained at Ψ_{min} and Ψ_{max} wavelengths for 25°. The calculated phase change at Ψ_{min} and Ψ_{max} is 140° and 178°, respectively. It confirms that dual-phase singularity at a single lower incident angle is possible with optical Tamm states. Moreover, the phase singularity at Ψ_{max} decreases with increasing incident angle (also see Supporting Information Fig. S4). This is because the Ψ_{max} value decreases with increasing incident angle. Moreover, the phase singularity spectral band broadens with increasing incident angle, especially the phase change at Ψ_{min} significantly blue shifts. The calculated spectral bandwidth ($\Delta\lambda = \lambda_{\Psi max}-\lambda_{\Psi min}$) of dual-phase singularity at 20° and 70° is 20 nm and 100 nm, respectively. The observed broadening of the phase singularity spectral band is due to the significant blue shift of p-polarized TPP resonance with increasing incident angle (Fig. 1c). As a result, dual-phase singularity is only visible at lower incident angles (<30°).

3 Experimental Demonstration of Dual-Phase Singularity

The designed TPP cavity is fabricated using physical vapor deposition techniques (see Supporting Information). Initially, Au film with a thickness of ~28 nm is deposited on cleaned Si wafers, followed by the deposition of ten alternating layers of Sb_2S_3 and SiO_2 with a thickness of ~180 nm and ~100 nm, respectively. In **Figure 2a**, we display the cross-sectional scanning electron microscope (SEM) image of the fabricated TPP cavity, where the numbers 1 to 10 represent the corresponding alternating layers of SiO_2 and Sb_2S_3. A variable angle spectroscopic ellipsometer with a minimum incident angle limit of 25° is used to obtain the polarized angular reflectance and ellipsometer parameters (Ψ and Δ). **Figures 2b** and **2c** show the measured angular reflectance (25° to 50°) for *s*-and *p*-polarization, respectively. As observed in the calculated results, measured data also shows that narrow linewidth TPP mode slightly blue shifts with increasing incident angle for *s*-polarization, and there is a significant blue shift of TPP resonance with linewidth broadening when the incident angle increases for *p*-polarization. However, both polarizations do not realize reflection zero at the TPP resonance wavelength. The increase in reflection amplitude at TPP resonance can primarily be attributed to the inherent surface roughness of the film and the variations in the individual thickness of the fabricated thin film, especially the thickness of Au and Sb_2S_3 termination layer. Note that a slight variation in the thickness of the Au layer and Sb_2S_3 termination layer can significantly change the Ψ_{min} and Ψ_{max} values (see Supporting Information Fig. S5). Therefore, the experiment considers the minimum reflection amplitude obtained for *p*-and *s*-polarization as Ψ_{min} and Ψ_{max}, respectively.

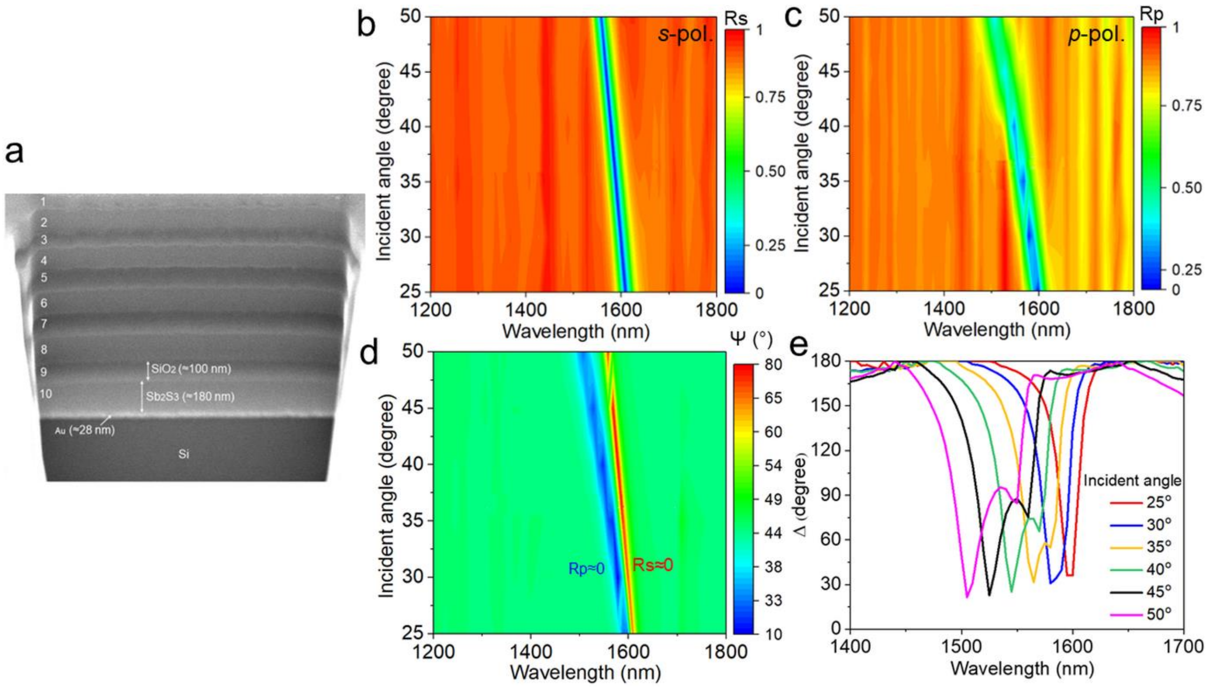

Figure 2. **Experimental validation of dual-phase singularity**. (**a**) The cross-sectional SEM image of the fabricated TPP cavity consists of ten alternating layers of SiO_2 and Sb_2S_3 with an Au layer of thickness ~28 nm at the bottom. Measured angular (25° to 50°) reflectance spectra for (**b**) *s*-polarization and (**c**) *p*-polarization. Measured ellipsometer parameters as a function of incident angle (25° to 50°) for (**d**) Ψ spectra and (**e**) Δ spectra.

As shown in **Figure 2d**, the measured Ψ_{min} and Ψ_{max} regions are obtained at the TPP resonance wavelength of *p*- and *s*-polarization, respectively, and both regions spectrally separate with increasing incident angle. **Figure 2e** shows the measured phase difference (Δ) spectra as a function of incident angle. As can be seen, a dual-phase singularity (one at Ψ_{min} and the second at Ψ_{max}) is realized at a lower incident angle of 25° and the phase change at Ψ_{max} decreases with increasing incident angle. The measured incident angle-dependent Δ response correlates well with the calculated results. We further investigated the influence of Au layer thickness on the dual-phase singularity and confirmed that an optimum Au layer thickness is required to achieve a dual-phase singularity with maximum phase change at Ψ_{min} and Ψ_{max} (see Supporting Information Fig. S6). It emphasizes that a narrow linewidth TPP mode (FWHM ≤40 nm) with reflection zero for both p-and s-polarization is required to realize dual-phase singularity at a single lower incident angle. Moreover, an inverse design algorithm [33] is recommended to achieve the π phase shift at both Ψ_{min} and Ψ_{max} since many structural parameters and incident angle must be optimized simultaneously.

4 Dual-Phase Singularity-based Ultra-Sensitive Hydrogen Sensor

We propose a TPP cavity-based scalable sensing platform for the ultra-sensitive detection of hydrogen (H_2) using the concept of dual-phase singularity. As a carbon-free energy vector, H_2 gas is a promising replacement for fossil fuels because its only by-product is water when consumed. However, H_2 is highly flammable with low ignition energy at ambient temperature and pressure for concentrations ranging from 4 to 75%. Consequently, H_2 sensing is an important safety issue in industries where H_2 is a crucial component or a by-product. Therefore, it is important to develop efficient and reliable H_2 sensors to detect H_2 concentrations ranging from a few tens of parts per billion (ppb) to a few percent under different environmental conditions[49]. In general, photonic-based H_2 sensors measure changes in the refractive index of the sensing materials that form hydrides upon exposure to H_2[50, 51]. They are hydride-based refractometers, most commonly using palladium (Pd). When Pd is exposed to H_2, it forms palladium hydride, PdH_x, which has a different complex refractive index than Pd depending on the H_2 stoichiometry, x. The lattice constant of Pd also changes with H_2 exposure[49].

The schematic of the proposed TPP-cavity to realize dual phase singularity for H_2 sensing is shown in the inset of **Figure 3a**. Tamm resonance can be excited by depositing the metal on either top or bottom of the DBR but with the metal layer on the high refractive index layer. For sensing application, the metal layer is preferred to be on top of the DBR, and a thin Pd layer (7 nm thick) is coated on the Sb_2S_3-SiO_2 DBR, where the thickness of Sb_2S_3 and SiO_2 is 180 nm and 100 nm, respectively. In this TPP cavity, the metal layer is coated on top of the DBR because the hydrogen can be directly exposed to the Pd layer. The thickness of the Sb_2S_3 termination layer (below Pd) is set to 160 nm. It is noted that the complex refractive index (n and k) of Pd changes with H_2 exposure. In particular, the complex refractive index contrast between Pd and PdH_x increases as wavelength increases from visible to NIR wavelengths[50]. Thus, a higher sensitivity is expected for a sensor operating at NIR wavelengths. As shown in Figure 3a, the designed TPP cavity shows a dual-phase singularity in the NIR wavelengths at a lower incident angle of 20°. The operation principle of the proposed hydrogen sensor is that the reversible transformation of Pd to PdH_x changes the reflected intensity at the TPP resonance wavelength due to changes in the Pd optical constants. This small change in intensity is transformed into a significant change in the reflected phase only at the dual phase singularity region.

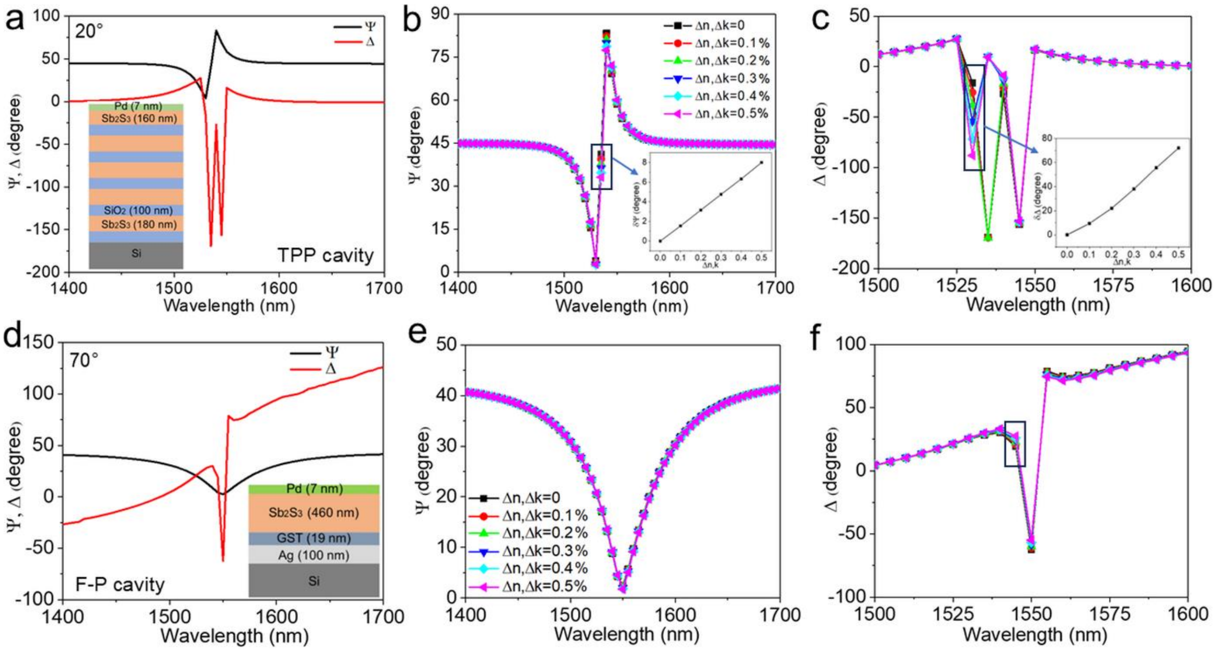

Figure 3. **Demonstration of the TPP-cavity-based ultra-sensitive hydrogen sensor.** (**a**) Calculated ellipsometer parameters of TPP cavity at an incident angle of 20°. A Schematic of the Pd-based TPP cavity for hydrogen sensing is shown in the inset of (a). The variation of ellipsometer parameters of TPP cavity with change in the complex refractive index of Pd (**b**) Ψ spectra, and (**c**) Δ spectra. The change in ellipsometry parameters with a change in the refractive index of Pd from 0.1 to 0.5% is shown in the inset of (b) for δΨ and (c) for δΔ. (**d**) Calculated ellipsometer parameters of F-P cavity at an incident angle of 70°. A Schematic of the Pd-based F-P cavity for hydrogen sensing is shown in the inset of (d). The variation of ellipsometer parameters of F-P cavity with change in the complex refractive index of Pd (**e**) Ψ spectra, and (**f**) Δ spectra.

In our calculations, the frequency-dependent complex refractive indices of Pd are taken from Werner et al.[52] and assumed that a small percentage (0.1 to 0.5 %) change in complex refractive index occurs when the H_2 atomic ratio increases continuously in Pd with H_2 exposure. To compare the sensing performance, we further propose a Pd-based F-P cavity made up of multilayer thin films of Pd (7 nm), Sb_2S_3 (460 nm), $Ge_2Sb_2Te_5$ (19 nm), and Ag (100 nm), as shown in the inset of **Figure 3d**. It is known that this type of asymmetric F-P cavity exhibits extreme phase singularity at a higher angle of incidence due to the presence of a thin lossy $Ge_2Sb_2Te_5$ layer [53, 54]. As shown in **Figure 3d**, the Pd-based F-P cavity shows phase singularity at an incident angle of 70° around the same wavelength. Here, the crystalline phase of $Ge_2Sb_2Te_5$ is used to achieve phase singularity at NIR wavelengths (see Supporting Information Fig. S7). Also note that the same thickness of the Pd layer is used in both configurations.

The calculated ellipsometry parameter, Ψ, with a change in the complex refractive index of Pd from 0 to 0.5 % is shown in **Figures 3b** and **3e** for the TPP cavity and F-P cavity, respectively. In contrast to the F-P cavity, a considerable change in Ψ is observed at a specific wavelength between the minimum and maximum value of Ψ in the TPP cavity. The corresponding calculated Δ spectra for the TPP cavity and F-P cavity are shown in **Figures 3c** and **3f**, respectively. Notably, a significant Δ shift with a change in the complex refractive index of Pd (0.1 to 0.5%) is obtained at the dual-phase singularity wavelength for the TPP cavity, while a small variation is observed at the single-phase singularity wavelength for the F-P cavity. We then calculated the change in ellipsometry parameters (δΨ and δΔ) with an increase in the complex refractive index of Pd from 0.1 to 0.5% and the same is shown in the inset of Fig. 3b and 3c for δΨ and δΔ, respectively. The linear variation of δΨ and δΔ reveals that both Ψ and Δ can be considered as a potential sensing parameter for dual-phase singularity to detect extremely small refractive index changes. The calculated phase sensitivity ($\delta\Delta/\delta n$) is 33,571°/RIU and 6250°/RIU for dual-phase singularity and single-phase singularity, respectively. It shows that the sensitivity of dual-phase singularity is five times higher than that of single-phase singularity. Here, the phase sensitivity is calculated by only considering the real parts of the refractive index ($\delta n = n_{Pd} - n_{0.1\%Pd}$). Also, the achieved detection limit is much higher compared to existing Tamm cavity-based hydrogen sensors [55, 56]. The proposed TPP cavity could be a potential scalable sensing platform to detect ultra-low concentrations of hydrogen. The proposed hydrogen sensor can be experimentally verified by using a microfluidic channel integrated Tamm cavity [53, 54] and an ellipsometer [50] or an interferometer-based differential phase measurement setup [57].

5 Spectrally Tunable Dual-Phase Singularity

To realize the equal phase change at the dual-phase singularity wavelengths for a spectral band, a continuously tunable zero-reflection TPP mode with the same linewidth is required. However, the aforementioned tunable TPP cavity (Fig.1) cannot provide this feature due to the linewidth broadening of TPP mode and the failure to achieve zero reflection for the crystalline Sb_2S_3 (see Supporting Information Fig. S2). In this context, we propose a metal-free Tamm cavity to realize spectrally tunable dual-phase singularity. **Figure 4a** shows the schematic of the proposed Tamm cavity consisting two DBRs made up of Sb_2S_3 and SiO_2 layers with thicknesses of 110 nm and 200 nm, respectively. DBR1 and DBR2 comprise 5 layers and 6 layers, respectively, and the thickness of the Sb_2S_3 termination layer in both DBRs is 158 nm.

In this cavity, the lossless interface mode or Tamm mode is excited at the boundary between the two DBRs and decays exponentially into both of them[58]. In **Figure 4b**, we show the excited Tamm mode at normal incidence for both amorphous and crystalline phases of Sb_2S_3. The simulated intensity distribution at the resonance wavelength of 1495 nm shows that the maximum field is confined at the Sb_2S_3 termination layer of two DBRs and decays exponentially in the surrounding media (see Supporting Information Fig. S8). It is important to note that zero-reflection mode with almost the same linewidth (FWHM≈36 nm) is achieved for both phases of Sb_2S_3. More importantly, a significant wavelength shift of 240 nm is obtained by changing the phase of Sb_2S_3 from amorphous to crystalline.

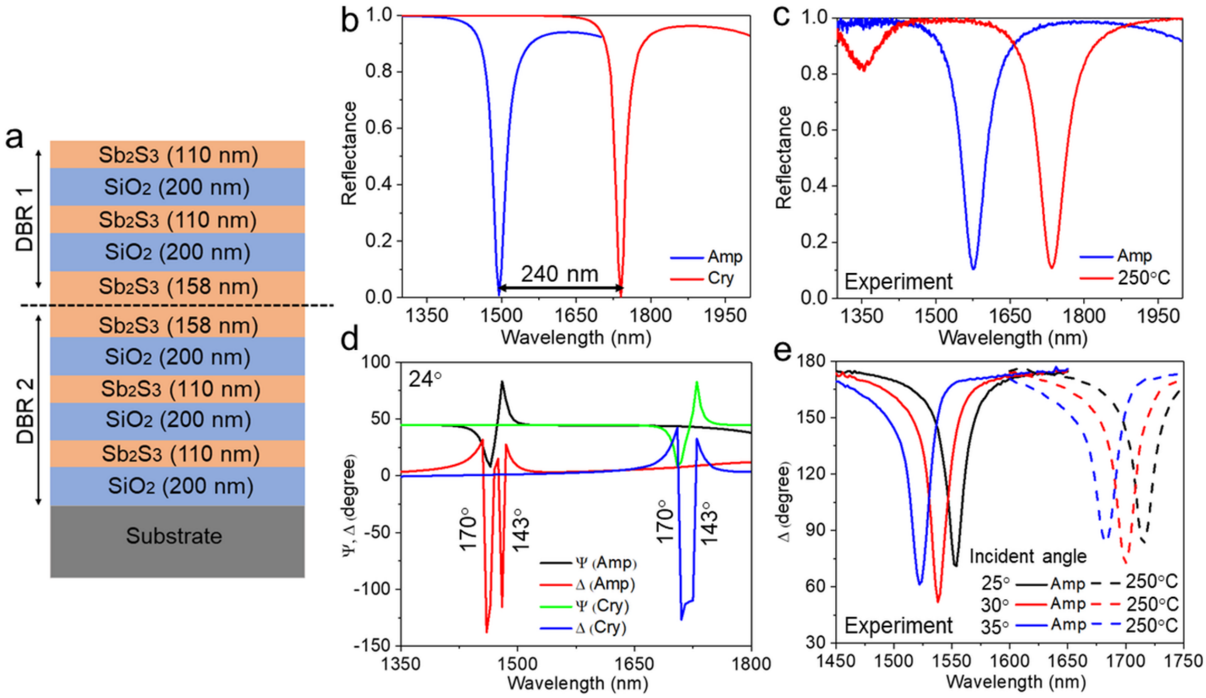

Figure 4. **Tunable dual-phase singularity using a metal-free Tamm cavity**. (a) Schematic of the designed Tamm cavity consisting of two DBRs made up of Sb_2S_3 and SiO_2 layers. The normal incidence reflectance spectrum for amorphous and partially crystallized cavities (b) Calculated and (c) Measured. (d) The pair of ellipsometer parameters (ψ and Δ) calculated at 24° for amorphous and crystalline phases of Sb_2S_3. (e) Measured Δ spectra for three incident angles (25° to 35°) for amorphous and partially crystallized cavities.

In the experiment, a SiO_2 capping layer with a thickness of 20 nm is deposited on top of the cavity to avoid the oxidation of the top Sb_2S_3 layer during the crystallization annealing process to minimize the surface roughness of the annealed cavity. Note that adding a 20 nm SiO_2 layer on top of the cavity will not change the Tamm resonance wavelength and amplitude (see Supporting Information Fig. S9). **Figure 4c** shows the measured normal incident reflectance spectrum of the cavity for amorphous and partially crystallized (annealed at 250°C) phases of Sb_2S_3. The polycrystalline features of annealed Sb_2S_3 are confirmed using Raman spectroscopy [59, 60] and X-ray diffraction (XRD) [61] (see Supporting Information Fig. S10). As can be seen, equal amplitude Tamm mode required for tunable dual-phase singularity is obtained in both phases of Sb_2S_3. The measured wavelength shift is 156 nm. The non-zero reflection and smaller spectral shift achieved in the experiment as compared to the simulation are due to the variations in the individual thickness of the fabricated cavity, the inherent surface roughness of the film, and partial crystallization of Sb_2S_3. Also, the angle-dependent *s*- and *p*-polarized reflectance spectra show that zero-reflection and narrow linewidth mode for both phases of Sb_2S_3 is possible only at lower incident angles (see Supporting Information Fig. S11 and Fig. S12). It indicates that this cavity also exhibits dual-phase singularity at lower incident angles.

Figure 4d shows the calculated pair of ellipsometer parameters (ψ and Δ) at 24°. Calculated phase change at Ψ_{min} and Ψ_{max} wavelengths for amorphous and crystalline phases is ≈170° and ≈143°, respectively. It shows that similar ψ spectra with the same phase change are obtained at the dual-phase singularity wavelengths by changing the phase of Sb_2S_3 from amorphous to crystalline. It shows that the continuous tuning of dual-phase singularity wavelength with the same phase change is possible within the tunable wavelength range. In **Fig. 4e**, we show the measured phase spectra at different incident angles (25° to 35°) for both amorphous and partially crystallized phases of Sb_2S_3. It is evident that the tunable dual-phase singularity is obtained for this angular range and a maximum phase change is realized at an incident angle of 30° for both phases of Sb_2S_3. In comparison to an amorphous cavity, a slightly lower phase change is obtained for a partially crystallized cavity due to the increased linewidth of the mode. Also, the experimentally measured dual-phase singularity angle (30°) is slightly higher than the calculated incident angle (24°). The multi-state forward tuning of dual-phase singularity is possible by continuously annealing the cavity electrically[62] or optically[60]. This multi-state spectrally tunable dual-phase singularity can find application in flat optics, especially to realize multispectral spatial light modulators [30].

6 Conclusion

In summary, we experimentally demonstrated optical Tamm state-induced dual-phase singularity at a single incident angle using a tunable TPP cavity consisting of an ultra-low loss Sb_2S_3 PCM as the active layer of the cavity. By exciting the Tamm modes in the NIR wavelengths for *s*- and *p*-polarizations of incident light at the same incident angle, we achieved a dual-phase singularity at the zero reflectance wavelengths at a lower incident angle, which is not possible with Fabry-Pérot cavities. Moreover, we demonstrated an ultra-sensitive hydrogen sensor by exploiting the concept of dual-singularity realized in a Pd-based TPP cavity. Compared to the single phase-singularity-based sensor, the proposed sensor can detect extremely small refractive index changes of the Pd layer due to hydrogen exposure through the dual phase singularity approach. Also, note that phase-sensitive detection is suitable for imaging with great potential to enable high throughput scalable hydrogen sensors. We further proposed a tunable Tamm cavity comprising two DBRs and experimentally demonstrated that spectral tunable dual-phase singularity is possible at lower incident angles. A significant wavelength shift of 240 nm with the same phase change is obtained at the dual-phase singularity wavelengths for the amorphous and crystalline phases of Sb_2S_3.

Supporting Information

Supporting Information is available from the Wiley Online Library or the authors.

Acknowledgements:

J. T. acknowledges funding support from the National Research Foundation Singapore under the CRP program (Grant No. NRF-CRP26-2021-0004). The authors R. S and S. J. acknowledge the funding support from the Ministry of Education (MOE), Singapore (Grant No: MOE-T2EP50121-0009).

Conflict of Interest

The authors declare no conflict of interest.

Data Availability Statement

The data that support the findings of this study are available from the corresponding author upon reasonable request.

References

[1] M. S. Soskin, M. V. Vasnetsov, *Prog. Opt.* **2001**, 42, 219

[2] K. V. Sreekanth, S. Sreejith, S. Han, A. Mishra, X. Chen, H. Sun, C. T. Lim, R. Singh, *Nat. Commun*. **2018**, 9, 369

[3] D. Hoenig, D. J. Moebius, *Phys. Chem.* **1991**, 95, 4590–4592

[4] K. V. Sreekanth, P. Mahalakshmi, S. Han, M. S. Mani Rajan, P. K. Choudhury, R. Singh, *Adv. Opt. Mater*. **2019**, 7, 1900680

[5] E. Cusworth, V. G. Kravets, A. N. Grigorenko, *ACS Photonics.* **2023**, 10, 3715–3722

[6] M. Liu, C. Zhao, Y. Zeng, Y. Chen, C. Zhao, C.-W. Qiu, *Phys. Rev. Lett*. **2021**, 127, 266101

[7] V. Maslova, P. Lebedev, D. G. Baranov, *Adv. Opt. Mater*. **2024**, 12, 2303263

[8] M. Li, L. Michaeli, H. A. Atwater, *ACS Photonics* **2024**, 11, 3554–3562

[9] G. Ma, W. Shen, D. S. Sanchez, Y. Yu, H. Wang, L. Sun, X. Wang, C. Hu, *ACS Nano* **2023**, 17, 17751–17760

[10] M. Liu, W. Chen, G. Hu, S. Fan, D. N. Christodoulides, C. Zhao, and C.-W. Qiu, *Phys. Rev. B* **2023**, 107, L241403

[11] A. Berkhout, A. F. Koenderink, *ACS Photon.* **2019**, 6, 2917–2925

[12] K. V. Sreekanth, C. M. Das, R. Medwal, M. Mishra, Q. Ouyang, R. S. Rawat, K. T. Yong, R. Singh, *Adv. Mater.* **2021**, 33, 2006926

[13] A. N. Grigorenko, P. I. Nikitin, A. V. Kabashin, *Appl. Phys. Lett.* **1999**, 75, 3917

[14] K. V. Sreekanth, Q. Ouyang, S. Sreejith, S. Zeng, W. Lishu, E. Ilker, W. Dong, M. ElKabbash, Y. Ting, C. T. Lim, M. Hinczewski, G. Strangi, K. T. Yong, R. E. Simpson, R. Singh, *Adv. Opt. Mater.* **2019**, *7*, 1900081

[15] Y. Zhang, M. T. Phoo, Y. Foo, X. Li, Y. W. Lam, J. A. Zapien, *Laser Photonics Rev*. **2024**, 2300801

[16] K. V. Sreekanth, Q. Ouyang, S. Han, K. T. Yong, R. Singh, *Appl. Phys. Lett.* **2018**, 112, 161109

[17] F. Wu, V. G. Kravets, H. O. Arola, M. Soikkeli, K. Iljin, G. Kim, M. Kim, H. S. Shin, D. V. Andreeva, C. Neumann, M. Küllmer, A. Turchanin, D. De Fazio, O. Balci, V. Babenko, B.

Luo, I. Goykhman, S. Hofmann, A. C. Ferrari, K. S. Novoselov, A. N. Grigorenko, Sci. Rep. **2019**, 9, 20286

[18] K. V. Sreekanth, S. Han, R. Singh, *Adv. Mater.* **2018**, 30, 706696

[19] K. V. Sreekanth, T. Yu, *J. Opt.* **2013**, 15, 055002

[20] K. V. Sreekanth, P. Prabhathan, A. Chaturvedi, Y. Lekina, S. Han, S. Zexiang, E. H. Tong Teo, J. Teng, R. Singh, *Small* **2022**, 18, 2202005

[21] V. G. Kravets, F. Schedin, R. Jalil, L. Britnell, R. V. Gorbachev, D. Ansell, B. Thackray, K. S. Novoselov, A. K. Geim, A. V. Kabashin, A. N. Grigorenko, *Nat. Mater.* **2013**, 12, 304–309

[22] L. Malassis, P. Massé, M. Tréguer-Delapierre, S. Mornet, P. Weisbecker, P. Barois, C. R. Simovski, V. G. Kravets, A. N. Grigorenko, *Adv. Mater.* **2014**, 26, 324–330

[23] H. Song, N. Zhang, J. Duan, Z. Liu, J. Gao, M. H. Singer, D. Ji, A. R. Cheney, X. Zeng, B. Chen, S. Jiang, Q. Gan, *Adv. Opt. Mater.* **2017**, 5, 1700166

[24] A. I. Aristov, M. Manousidaki, A. Danilov, K. Terzaki, C. Fotakis, M. Farsari, A. V. Kabashin, *Sci. Rep* **2016**, 6, 25380

[25] J. P. Cuanalo-Fernández, N. Korneev, I. Cosme, M. B. de la Mora, J. A. Urrutia-Anguiano, A. Reyes-Coronado, R. Ramos-García, S. Mansurova, *J. Phys. Chem. C* **2024**, 128, 11372–11381

[26] W. Liu, J. Wang, Y. Tang, X. Wang, X. Zhao, L. Shi, J. Zi, C. T. Chan, *Nano Lett.* **2024**, 24, 943–949

[27] G. Ermolaev, K. Voronin, D. G. Baranov, V. Kravets, G. Tselikov, Y. Stebunov, D. Yakubovsky, S. Novikov, A. Vyshnevyy, A. Mazitov, I. Kruglov, et al. *Nat. Commun.* **2022**, 13, 2049

[28] P. A. Thomas, K. S. Menghrajani, W. L. Barnes, *Nat. Commun.* **2022**, *13,*1809

[29] Y. Zeng, R. Hu, L. Wang, D. Gu, J. He, S.-Y. Wu, H.-P. Ho, X. Li, J. Qu, B. Z. Gao, Y. Shao, *Nanophotonics* **2017**, 6, 1017-1030

[30] S. Mansha, P. Moitra, X. Xu, T. W. W. Mass, R. M. Veetil, X. Liang, S. Q. Li, R. Paniagua-Dominguez, *Light Sci Appl* **2022**, 11, 141

[31] M. Kaliteevski, I. Iorsh, S. Brand, R. A. Abram, J. M. Chamberlain, A. V. Kavokin, I. A. Shelykh. *Phys. Rev. B* **2007**, 76, 165415

[32] H.-C. Cheng, C.-Y. Kuo, Y.-J. Hung, K.-P. Chen, S.-C. Jeng, *Phys. Rev. Appl.* **2018**, 9, 064034

[33] M. He, J. R. Nolen, J. Nordlander, A. Cleri, N. S. McIlwaine, Y. Tang, G. Lu, T. G. Folland, B. A. Landman, J.-P. Maria, J. D. Caldwell, *Nat. Mater.* **2021**, 20, 1663–1669

[34] K. V. Sreekanth, J. Perumal, U. S. Dinish, P. Prabhathan, Y. Liu, R. Singh, M. Olivo, J. Teng, *Nat. Commun.* **2023**, 14, 7085

[35] W.-H. Xu, Y.-H. Chou, Z.-Y. Yang, Y.-Y. Liu, M.-W. Yu, C.-H. Huang, C.-T. Chang, C.-Y. Huang, T.-C. Lu, T.-R. Lin, K.-P. Chen, Adv. Photonics Res. **2020**, 3: 2100120

[36] M. He, J. Ryan N. J. Nordlander, A. Cleri, G. Lu, T. Arnaud, N. S. McIlwaine, K. Diaz-Granados, E. Janzen, T. G. Folland, J. H. Edgar, J. P. Maria, J. D. Caldwell. *Adv. Mater*. **2023**, 35, 2209909

[37] X. Tu, Y. Zhang, S. Zhou, W. Tang, X. Yan, Y. Rui, W. Wang, B. Yan, C. Zhang, Z. Ye, H. Shi, R. Su, C. Wan, D. Dong, R. Xu, Q. Y. Zhao, L. B. Zhang, X. Q. Jia, H. Wang, L. Kang, J. Chen, P. Wu, *Nat Commun* 2024, **15**, 5542

[38] Z.-Y. Yang, Z.-Y. Yang, S. Ishii, T. Yokoyama, T. D. Dao, M.-G. Sun, P. Pankin, I. Timofeev, T. Nagao, K.-P. Chen, *ACS Photon.* **2017**, 4, 2212–2219

[39] C. Symonds, G. Lheureux, J. P. Hugonin, J. J. Greffet, J. Laverdant, G. Brucoli, A. Lemaitre, P. Senellart, J. Bellessa, *Nano Lett.* **2013**, 13, 3179–3184

[40] C. Zhang, K.Wu, V. Giannini, X. Li, *ACS Nano* **2017**, 11,1719–1727

[41] W. L. Zhang, F. Wang, Y. J. Rao, Y. Jiang, *Opt. Exp.* **2014**, 22, 14524–14529

[42] S. Normani, P. Bertolotti, F. Bisio, M. Magnozzi, F. F. Carboni, S. Filattiera, S. Perotto, F. Marangi, G. Lanzani, F. Scotognella, G. M. Paternò, *ACS Appl. Mater. Interfaces*. **2023**, 15, 27750–27758

[43] B. Auguié, M. C. Fuertes, P. C. Angelomé, N. L. Abdala, G. J. A. A. Soler Illia, A. Fainstein, *ACS Photonics* **2014**, 1, 775– 780

[44] Y. Tsurimaki, J. K. Tong, V. N. Boriskin, A. Semenov, M. I. Ayzatsky, Y. P. Machekhin, G. Chen, S. V. Boriskina, *ACS Photon.* **2018**, 5, 929–938

[45] S. V. Boriskina, Y. Tsurimaki, *Journal of Physics: Condensed Matter* **2018**, *30*, 224003

[46] P. Prabhathan, K. V. Sreekanth, J. Teng, J. H. Ko, Y. J. Yoo, H. H. Jeong, Y. Lee, S. Zhang et al., *iScience* **2023**, 26, 107946

[47] K. V. Sreekanth, S. Jana, M. ElKabbash, R. Singh, J. Teng, *Nanophotonics* **2024**, 13, 2075-2088

[48] P. Yeh, A. Yariv, C. S. Hong, *J. Opt. Soc. Am.* **1977**, 67, 423–438

[49] I. Darmadi, F. A. A. Nugroho, C. Langhammer, *ACS Sensors* **2020**, 5, 3306−3327

[50] M. ElKabbash, K. V. Sreekanth, Y. Alapan, M. Kim, J. Cole, A. Fraiwan, T. Letsou, Y. Li, C. Guo, R. M. Sankaran, U. A. Gurkan, M. Hinczewski, G. Strangi, *ACS Photon.* **2019**, 6, 1889

[51] F. A. A. Nugroho, I. Darmadi, L. Cusinato, A. Susarrey-Arce, H. Schreuders, L. J. Bannenberg, A. B. Da Silva Fanta, S. Kadkhodazadeh, et al., *Nat. Mater*. **2019**, 18, 489−495

[52] W. S. M. Werner, K. Glantschnig, C. Ambrosch-Draxl, *J. Phys Chem Ref. Data* **2009**, 38, 1013-1092

[53] K. V. Sreekanth, S. Sreejith, Y. Alapan, M. Sitti, C. T. Lim, R. Singh, *Adv. Opt. Mater*. **2019**, 7, 1801313

[54] A. R. Rao, K. V. Sreekanth, S. Sreejith, V. Jose, S. Pethe, R. Singh, *Adv. Opt. Mater*. **2022**, 10, 2102623

[55] Y.-S. Chen, Z.-Y. Yang, M.-J. Ye, W.-H. Wu, L.-H. Chen, H.-J. Shen, S. Ishii, T. Nagao, K.-P. Chen, *Adv. Phys. Res*. **2023**, 2, 2200094

[56] K. Zhang, Z. Chen, H. Li, Z. Yi, Y. Liu, X. Wu, *Phys. Chem. Chem. Phys.*, **2023**, 25, 20697-20705

[57] S. Zeng, K. V. Sreekanth, J. Shang, T. Yu, C.-K. Chen, F. Yin, D. Baillargeat, P. Coquet, H.-P. Ho, A. V. Kabashin, K.-T. Yong, *Adv. Mater*. **2015**, 27, 6163-6169.

[58] A. V. Kavokin, I. A. Shelykh, G. Malpuech, *Phy. Rev. B* **2005**, 72, 233102

[59] O. A. M. Abdelraouf, X. C. Wang, C. H. Goh Ken, C. B. Lim Nelson, S. K. Ng, W. D. Wang, X. Renshaw Wang, Q. J. Wang, H. Liu, *Adv. Photonics Res*. **2023**, 4, 2300209

[60] S. Jana, K. V. Sreekanth, O. A. M. Abdelraouf, R. Lin, H. Liu, J. Teng, R. Singh, *Nano Lett.* **2024**, 24, 3922–3929

[61] Y. Gutiérrez, A. Fernández-Pérez, S. A. Rosales, C. Cobianu, M. Gheorghe, M. Modreanu, J. M. Saiz, F. Moreno, M. Losurdo, *Opt. Mater. Express* **2022**, 12, 1531-1541

[62] P. Prabhathan, K, V. Sreekanth, J. Teng, R. Singh, *Nano Lett.* **2023**, *23*, 5236–5241

ToC Summary

Realizing multiple-phase singularities is important for phase engineering in flat optics, and to improve the detection limit of refractive index sensors. The existence of a dual-phase singularity at a single incident angle with spectral tunability and its application for ultra-sensitive hydrogen sensing is presented using phase change material-based tunable Tamm plasmon polariton cavities.

ToC Image